HHS Public Access

Author manuscript

IEEE Access. Author manuscript; available in PMC 2024 July 18.

Published in final edited form as:

IEEE Access. 2024 ; 12: 89613–89620. doi:10.1109/access.2024.3416869.

Stretching the Limits of MRI—Stretchable and Modular Coil Array Using Conductive Thread Technology

FOLK W. NARONGRIT[1,2] **[Member, IEEE]**, **THEJAS VISHNU RAMESH**[2] **[Member, IEEE]**, **JOSEPH V. RISPOLI**[1,2,3] **[Member, IEEE]**

[1]Elmore Family School of Electrical and Computer Engineering, Purdue University, West Lafayette, IN 47907, USA

[2]Weldon School of Biomedical Engineering, Purdue University, West Lafayette, IN 47907, USA

[3]Department of Radiology and Medical Imaging, University of Virginia, Charlottesville, VA 22903, USA

Abstract

Objective: We propose a modular stretchable coil design using conductive threads and commercially available embroidery machines. The coil design increases customizability of coil arrays for individual patients and each body part.

Methods: Eight rectangular coils were constructed with custom-fabricated stretchable tinsel copper threads incorporated onto textile. Tune, match, and detune circuits were incorporated on the coil. A hook-and-loop mechanism was used to attach and decouple the modular coils. Phantom and *in vivo* scans at various anatomical flexion angles were acquired to highlight performance, and a temperature test was performed to verify safety.

Results: *In vivo* MRI experiments demonstrate high sensitivity and coverage of each anatomy. As the coils are stretched, the sensitive volume increases at a rate of 10.93 mL/cm^2. The SNR reduction of a single coil was greater during compression than when stretched, but this did not affect image quality for the array. The modularity of the array allows for adaptability for any anatomy with simple on-demand adjustment to the number and position of coil elements.

Conclusion: The images demonstrated high sensitivity and coverage of the stretchable array for various anatomies and flexion angles. Stretching the coils increases the sensitive volume, allowing for a larger region to be effectively imaged. The resonance shift and SNR decrease during stretch and compression support further investigation of methods to reduce frequency shift in stretchable coils.

Significance: The proposed array design allows for highly stretchable, flexible, modular, and conformal patient-centered coils that allow for increased imaging quality, greater comfort, and rapid production.

Corresponding author: Joseph V. Rispoli (jvr4a@virginia.edu).

INDEX TERMS

Biomedical imaging; electromagnetic devices; flexible electronics; magnetic resonance imaging; radiofrequency coils; stretchable electronics

I. INTRODUCTION

Magnetic resonance imaging (MRI) is a non-invasive medical imaging modality that provides unparalleled soft tissue contrast and functional data [1]. The standard MRI involves placing the patient in a static magnetic field (B0), which induces a net magnetic moment. Radiofrequency (RF) pulses are emitted to excite the magnetization, which emits small amounts of RF signal at the characteristic resonant frequency of the desired element (e.g., hydrogen, sodium) proportional to the magnetic field. This signal is detected from receive coils placed close to the body over the desired imaging region. The receive coils work by Faraday induction with the body and pass analog coded information to be amplified, digitized, and reconstructed. Multiple gradient waveforms in three-dimensional space allow for encoded spatial information that sets the spatial resolution of the resulting image [2]. The gradient switching time ultimately sets the MRI scan time.

MRI acquisition is fundamentally slow and has signal-to-noise ratio (SNR) limitations. The resultant image quality and spatial resolution are limited and are prone to motion artifacts due to long acquisition times. Modern advances such as parallel imaging and advanced reconstruction techniques reduce the scan time but are still limited by the SNR obtained using shorter scan time. SNR can be increased using ultra high field (UHF) scanners and contrast agents which poses additional challenges [3]. Using better receive coil designs provide a less costly alternative with significant SNR gain.

Surface receive coils are built to acquire images with the highest SNR for a specific anatomical region of the body [4]. Commercial surface coils are typically manufactured using high-quality electronic components, thick copper traces, and low-loss substrates. In addition, the coils are packaged using medical-grade material that meets regulatory requirements, contributing to the arrays' size, weight, and flexibility. Commercial surface coils are produced to accommodate a range of anatomies and dimensions, increasing the mean offset distance between the coil and anatomy, which reduces the available SNR [5] (Fig. 1). This problem is especially prominent when using the same coils designed for adults in children [6]. If a surface coil array designed for adults is used in children, there would be larger gaps between the coil elements and the desired anatomy.

Another challenge in using conventional surface coils is their use on anatomies with flexion and curved anatomies such as the neck, knee, or elbow. Conventional coils do not fit perfectly against these anatomies, reducing SNR compared to coils that perfectly fit the curved anatomy [5]. When the receive coil is placed flush to the body with minimal gaps, its sensitivity to the RF signal is significantly increased. Highly flexible receive RF coils [6], [7], [8], [9], [10], [11], [12] have been the focus of research offering relatively rigid yet bendable solutions to the SNR problem. Although the SNR problem with curved anatomies has been partially solved with these designs, MRI coils with full adaptability to

all anatomies require coils to be highly conformable. Prototypes that address this issue have employed liquid metal [2], [13], conductive braids [14], and coated threads [15].

We have previously reported a stretchable two-channel receive coil prototype using a conductive thread on an athletic fabric [15], [16], which was fabricated using manual sewing machine stitching. That design is lightweight and omnidirectionally stretchable with up to 26% stretchability [16], addressing the issues mentioned earlier. The purpose of that study was to understand the decoupling performance of overlapped conductive thread receive coils for various stretch configurations. The latest work from our group used the embroidery machine to fabricate a stretchable coil for small animals at 7 T [17]. These works provide feasibility and motivation for a modular stretchable conductive thread coil for applications at 3 T.

We report a modular approach to stretchable receive array design that uses an easily fabricated conductive thread and a commercially available embroidery machine to produce consistent and customized coils quickly. This work applies results from our previous works to develop a modular coil array that minimizes mutual coupling effects. Innovations in flexible printed circuit boards (PCB) and the use of commonly available textile fabrics allow our design to be fully stretchable yet cost-effective. To our knowledge, this work represents the first modular stretchable surface coil using conductive threads. The modularity allows the number of channels, hence the effective coil size, to be changed on demand. Furthermore, our method addresses SNR limitations by having flexible, comfortable, and lightweight receive coil components that are closely fitted and conforms to curved surfaces of the human body, like bespoke garments, without restricting the patient inside a conventional coil's shell.

II. MATERIALS AND METHODS

A. COIL DESIGN AND FABRICATION

Eight rectangular coils with dimensions 100 mm × 50 mm were constructed with custom-fabricated stretchable tinsel copper threads (C3406G22YA, Maeden Innovation, Taiwan). The threads have an outer diameter of 0.32 mm, a linear resistance per unit length of 1.43 Ω/m, a break load of 40.31 N, and a maximum elongation of 3.2%.

The threads were embroidered on 81% 40/34 Nylon, 19% 40 denier spandex Tricot fabric (7KW18XST, The Moore Company, Rhode Island, USA) with a stretch of 150%. Stitching was done on the Innovis VE2200 embroidery machine (Brother Industries Ltd., Nagoya, Japan. The dimensions of the loop were chosen based on average anatomy circumference data [18], [19] to provide the maximum SNR penetration (90 mm) for 95% of the population using the quasistatic approximation method derived by Kumar et al. [20]; this approximation is given as

$$r = \frac{d}{\sqrt{5}} \tag{1}$$

for images at depth d and a circular coil of radius r. A rectangular coil with the same area as the circular coil would have the same maximum SNR [21]. A comparison coil was etched on to a 1-oz copper-clad FR-4 (0.2-mm thickness) printed circuit board (PCB) with the same dimensions as the unstretched coil.

The schematic and implementation of our stretchable coil is shown in Fig. 2. The coils were segmented on opposite sides of the conductor for the attachment of matching and tuning components. A flexible printed circuit board (PCB) containing tuning capacitors was placed in series between one segment gap and functions to set the correct resonant frequency of 127.8 MHz (the Larmor frequency of proton at 3 T). Another PCB on the opposite gap was added to the coil, containing matching capacitors that transforms the impedance of the coils to the characteristic impedance of 50 Ω. The matching network incorporates a compact LC lattice balun for transmission line matching [22], [23]. Non-magnetic multilayer ceramic capacitors (1111P, Passive Plus Inc., New York, USA) were used as the tuning and matching elements. A PIN diode (MA4P7006F, MACOM, Massachusetts, USA) and a series inductor (1008CS, Coilcraft, Illinois, USA) were placed in parallel to the tuning capacitor, deactivating the coils during the transmit phase.

Each coil was individually tuned and matched with the imaging phantom using an S_{11} measurement on the network analyzer (E5071C, Keysight Technologies, California, USA). The tuning and matching capacitor values were iteratively selected until each coil resonated at the Larmor frequency with a 50Ω impedance.

Individual coil elements were decoupled and attached using hook-and-loop fasteners. The amount of coil overlap was determined by connecting each pair of adjacent coils to the network analyzer. The coil overlap was adjusted until $|S_{21}|$ between the coil was minimized. The hook-and-loop fasteners were placed such that the stretchability is not affected. In addition, the fasteners provide a mechanism for coil channels to be added and removed as needed, allowing for modularity without affecting coil tuning or decoupling. A 3D-printed floating cable trap [22] was used to remove common-mode currents in the cable shields.

B. COIL CHARACTERIZATION AND BENCH TESTS

The coils were tested, tuned, and matched on the network analyzer. An in-house broadband decoupled probe was used to determine the coil quality factor (Q). The decoupled probe was decoupled in free space to a noise floor of −60 dB. Loaded and unloaded Q were computed as the ratio between the peak frequency to the 3-dB bandwidth of the insertion loss (S_{21}) [24]. Loaded (Q_{loaded}) and unloaded (Q_{unloaded}) quality factors were evaluated for the unstretched coil, ±10%, ±20%, ±30%, and ±40% uniform strains.

The unloaded quality factor Q_{unloaded} is a measure of the resistive losses of the coil and is measured in free space. The loaded quality factor Q_{loaded}, a measure of both the coil losses and sample losses, was measured by loading the coils with a cylindrical phantom (ε_r = 63.5, σ = 0.72S/m). Since the resonance frequency shifts due to the inductance change from stretching, Q was computed based on the respective resonance frequencies. The ratio between the Q_{loaded} and the Q_{unloaded} (Q ratio) is computed as an indicator of the coil sensitivity [25].

All network analyzer measurements were performed using 1601 points, centered at 128 MHz with a frequency span of 100 MHz. The velocity factor (0.66) of the measurement coaxial cables (RG174, Belden, Illinois, USA) and their electrical lengths were calibrated on the network analyzer prior to measurements. Proper care was taken to ensure coils and testing apparatus were at least 0.50 m away from conductive and magnetically susceptive materials to prevent artificial loading of the coil.

C. TEMPERATURE SAFETY TESTS

A temperature test experiment was performed on a cylindrical phantom to verify the compliance with the safety requirements set in IEC 60601-2-33:2022, Annex AA.1, subclause “Concerning 201.12.4.103.1 Limits of temperature” [26] and to address the possibility of tissue heating during RF transmission due to increased temperature of the coil elements heating [7]. The methodology used is the FDA-recognized consensus [27] standard NEMA MS 14–2019 [28], [29].

A 40-minute sequence (Spin echo, TR = 800 ms, TE=11 ms, 128 slices, slice thickness 1 mm, single-echo) at the First Level Controlled specific-absorption rate (SAR) limit was run for two different conditions: (1) Normal intended use configuration; (2) single-fault (unplugged coil); at two different positions: (1) isocenter (2) next to the bore wall at the isocenter plane; and at two load conditions: (1) loaded with a phantom; (2) with no load. There were eight testing configurations in total. In accordance with the standard, the sequence parameters were chosen to maximize the B_1 fields, which potentially maximizes coil heating.

A preliminary test scan was done to determine the locations with the highest temperature rise. After the scan was performed, a thermal image (ONE Pro, FLIR, OR, USA) of the coil was taken. Four fiber-optic temperature probes (OTG, Opsens Solutions, Québec, Canada) were connected to a signal conditioner (AccuSens, Opsens Solutions, Québec, Canada). The temperature probes were then connected to the locations with the highest temperature rise as determined by the thermal image. One temperature sensor was placed on the conductive thread, one on the tuning capacitor PCB, one on the matching PCB, and one on the non-conductive side of the fabric. The initial temperature of each probe at the start of the scan was calibrated to match the ambient temperature of the scanner room.

D. MRI EXPERIMENTS

The imaging experiments were performed on a Discovery MR750 3-Tesla MRI scanner (GE Healthcare, Illinois, USA). Image reconstruction was performed by the scanner with coil intensity correction and was unchanged from methods used in conventional coils.

For phantom experiments (Fig. 3a), the stretchable 8-channel coil was affixed to a 1.90-liter cylindrical phantom containing a solution of 3.75 g L^{-1} of $NiSO_4 \cdot 6H_2O$ and 5 g L^{-1} NaCl (Siemens AG, Munich, Germany). Images were acquired using the unstretched coil and coils with ±10%, ± 20%, ±30%, and ±40% omnidirectional strain, where the coil followed the curvature of the phantom. The coil fixture was connected via quarter-wavelength RG174 coaxial cables to a receiver gateway box (Clinical MR Solutions, Wisconsin, USA), which housed low-input impedance preamplifiers. The quarter-wavelength cables facilitated

preamplifier decoupling [25]. The coaxial cable contained a 3D-printed floating common-mode current trap [30] tuned to the Larmor frequency. The single-channel flexible FR-4 PCB coil was used as a benchmark for SNR comparisons; it was wrapped and taped directly on the phantom cylinder. For SNR measurements, a gradient echo sequence (axial, TR=400 ms, TE=1.86 ms, FOV=140 × 140 mm, slice thickness 2 mm, averages=1, tip angle 40°) was used.

SNR values were calculated using in-house code following method 4 of the NEMA MS 1–2008 (R2014, R2020) [31], which computes the ratio of the mean pixel value of signal within the region of interest divided by the standard deviation of the noise calculated in the background region of the image. The pixel-wise SNR maps were generated by dividing each pixel value by the standard deviation of the total standard deviation of the noise. The SNR penetration depth plot was computed by measuring the average SNR at each penetration depth.

Sensitive volume is defined as the volumetric region in which the coil's sensitivity (SNR) drops to 37% of that at the center of the coil and is the three-dimensional extension of penetration depth [25]. Sensitive volume can be computed using the equation:

$$V = \sum_{S \in Slices} (A_S \times \Delta x \times \Delta y \times T) \quad (2)$$

where V is the sensitive volume (cm^3), A_s is the sensitive area of each slice ($pixels^2$), Δx and Δy is the pixel size in each direction (cm/pixel), and T is the slice thickness (cm).

Scans from the SNR experiments are processed using in-house code on MATLAB R2022b (MathWorks, Massachusetts, USA). Each axial slice is passed through a masking threshold in which pixels of less than 37% intensity (relative to the center of the coil) are removed, resulting in a masked region of sensitivity (sensitive area). Spurious islands of noise outside the phantom region are filtered out such that the remaining pixels are inside of the phantom. The remaining pixels in one slice represent the sensitive area, which is then scaled to cm^2. Sensitive area of each slice is computed and combined to yield the sensitive volume. Fig. 4 demonstrates how the sensitive volume is computed.

In vivo testing was performed with approval from the Purdue University institutional review board (protocol 1903021919, approved March 23, 2022) and informed consent from the healthy male volunteer.

To highlight the SNR performance of the stretchable coils, high-resolution anatomical images were acquired from anatomies (knee, spine, and wrist) with varying degrees of flexion and curvature using the fast spin echo sequence (Fig. 3b–c). The coil was placed flush against the anatomy using hook-and-loop straps. For the wrist scans, four channels were removed, allowing for a closer fit to the anatomy.

III. RESULTS

A. COIL FABRICATION

Coil fabrication took 26 seconds per coil element. The fabrication process using embroidery machine allows rapid prototyping using different textile substrates and conductive threads without completely redesigning the manufacturing process. Additionally, the embroidery process allows customized manufacturing of receive coils in any shape or size required.

B. STRETCHABLE COIL PERFORMANCE AT DIFFERENT STRETCH LEVELS

The coil return loss ($|S_{11}|$) and resonance frequency were plotted against the amount of stretch to evaluate the coil's performance under stretch and compression, shown in Fig. 5. While the return losses were generally consistent for both stretch and compression (≈ −20 dB), the frequency shift was more prevalent when the coils were compressed. At the maximum stretch of 40%, the frequency shift of the proposed coil was −4.3 MHz (3.37%), and at the maximum compression of 40%, the shift was 8.8 MHz (6.89%).

The quality (Q) factor of the coils at every 10% omnidirectional stretch and compression is shown in Fig. 6. The maximum Q ratio, $Q_{unloaded}/Q_{loaded}$ was 2.36 when unstretched demonstrates that sample losses dominate coil losses. The copper reference coil has a Q ratio of 2.70.

Scans of the cylindrical phantom are shown in Fig. 7a. The respective SNR maps are shown in Fig. 7b. The SNR maps and penetration plots were normalized to the global maximum SNR of all the scans, and all images have been set to the same window level for comparison. The coils exhibited a 24% maximum SNR reduction for 40% stretch and a 30% SNR reduction for 40% compression. The reduction of SNR was greater when the coils were compressed than when stretched.

All coil configurations provided stable coil sensitivity up to the desired penetration depth of 90 mm, and no configuration yielded a sensitivity drop of less than 37% of the maximum value up to the desired penetration depth [25]. When compared to the copper reference coil with the same dimensions as the unstretched coil, the stretchable coils exhibit a 95–105% local SNR of the reference coil.

The sensitive volume for selected coil stretch and compression is shown in Fig. 8. A reconstruction of the sensitive volume is shown in Fig. 9. Separate best fit lines are shown separately for stress and compression. For stretch, the sensitive volume per unit coil area increased at a rate of 10.93 mL/cm^2, 95% CI [10.379, 11.488]. For compression, the sensitive volume per unit coil area increased at a rate of 25.4 mL/cm^2, 95% CI [12.622, 38.178]. The results indicate that stretching and compressing the coils changes the region that the coils can effectively image.

C. TEMPERATURE SAFETY TEST

A 40-minute scan was performed with the connected coil, and the temperature was continuously monitored using fiber-optic temperature probes. Fig. 10 shows the temperature of each coil component over the first 20 minutes of that scan. The temperature of all

components generally remained constant during the remainder of the scan. Temperatures at each location were verified to be less than 41 °C, and the maximum temperature rise after 20 minutes of scanning did not exceed 4 °C. The proposed coil meets the temperature requirements set under IEC 60601-2-33:2022.

D. IN VIVO IMAGING

Select spin echo anatomical images of the unbent knee, the knee at a 15- and 30-degree flexion angle, the wrist, and the spine are shown in Fig. 11. The knee and spine were imaged using the full eight channels, while only four channels were utilized for the wrist scan. The images demonstrated high sensitivity and coverage of the stretchable array. For knee scans, the image quality was generally unchanged when the knee is bent, indicating well-controlled tuning, matching, and decoupling of the coils. The volunteer was able to comfortably bend their knee at both 15° and 30° without removing the array.

IV. DISCUSSION

In this work, we present a fully functional 8-channel stretchable and modular coil array using conductive-thread technology. Our stretchable coils demonstrate that future developments in MRI coils can be personalized and custom-built for any anatomy to improve patient comfort and imaging quality for radiologists. While conventional coils have lower resistive losses and higher sensitivity compared to the current conductive-thread design, it is impractical and cost-prohibitive for conventional arrays to be custom-built for each patient. Further, it is often not clinically feasible for conventional coils' conductors to be closely wrapped to the anatomy being imaged, as was the case for the copper reference coil used for the phantom experiment. While regulatory laws do not currently allow for point-of-care manufacturing apart from discussion on 3D-printing at the point of care [32], [33], the rapid fabrication process using low-cost materials available in the market may provide future opportunities for healthcare facilities to produce tailored flexible coils in a matter of hours.

Our stretchable coil design addressed the limitations of conventional coils by having stretchable, comfortable, lightweight, and modular components that are closely fitted and conform to all surfaces of the body, providing similar or better image quality than conventional coils that do not closely fit the anatomy. A well-fabricated stretchable array can be put on by the patients themselves and adjusted for comfort, enhancing the experience of both the patient and the radiologist. While the overall SNR decreases when the coil is not at its unstretched position, the sensitive volume changes. This may be useful in certain applications such as for coil-based spatial localization in MR spectroscopy or imaging regions that have differing sizes among patients such as the breast or abdominal area.

The modular design of our stretchable array allows even greater adaptability and conformity. The number of coils can be added or removed through the use of hook-and-loop fasteners at locations pre-determined for optimal coil decoupling. A stretchable and modular surface coil provides the feasibility of customizing coil arrays for individual patients and each body part. This study demonstrated the proposed modular array for knee, spine, and wrist MR, but the

range of applications can be extended to head, ankle, abdominal, and other curved anatomies by rearranging the number and positions of coil elements.

There are several potential applications of our proposed design. Kinematic and dynamic MRI studies often employ specialized equipment that reduces the comfort of patients [13], [34]. Stretchable coils reduce the amount of equipment and increase comfort while providing better insights through higher coil sensitivity without restricting the patient through the coil shell or other equipment. Stretchable MRI coils may also provide insight into other applications of textile electronics, such as stretchable sensors or antennas.

The stretchability of the proposed design is limited by its least stretchable component, the sewed threads. While clinical applications do not require the coils to stretch beyond what is demonstrated in this work, it is critical to include a safety factor to prolong the life of the stretchable coils and to allow for occasional extreme stretches without failure. While using threads with a larger cross section may improve the Q ratio of the coil, the thickness of the threads is limited by the embroidery machine's ability to sew without fraying. Future work focuses on removing this limitation by optimizing the stitch patterns to balance between coil resistance (hence quality factor and SNR) and stretchability. Another limitation of our proposed design is the resonance frequency shift as the coil is stretched or compressed, reducing SNR. This effect is especially pronounced in coil compression, which may affect the quality of images of certain regions with high bending radius. In addition, the SNR and sensitive volume change due to stretch is more predictable than when compressed. Current research attempts to reduce the effect of this frequency shift through the use of interdigital capacitors [2], [35] or automatic tuning techniques [21], [36], [37]. Our future work focuses on optimizing and miniaturizing these techniques to allow for clinical use. As research in conductive thread technology continues to improve, reducing resistivity and increasing stretchability, stretchable coils will continue moving towards clinical viability.

V. CONCLUSION

In this work, we propose a stretchable RF coil design based on embroidered conductive thread technology. We demonstrate that imaging quality is not compromised for *in vivo* imaging of anatomies at various flexion angles. The proposed stretchable coil design offers an opportunity for highly stretchable, flexible, and conformal patient-centered coils that provide better SNR, allow for greater comfort, and can be rapidly produced.

Supplementary Material

Refer to Web version on PubMed Central for supplementary material.

ACKNOWLEDGMENT

The authors would like to thank Oni Chen and his team from Maeden Innovation Company Ltd., for their efforts in developing the novel conductive threads used in this work and also would like to thank Nathan Ooms R. T. (R)(MR) for his assistance with imaging.

This work was supported in part by the National Institutes of Health—National Institute of Biomedical Imaging and Bioengineering under Grant R03EB026231, and in part by the National Cancer Institute under Grant

P30CA023168. Publication of this article was funded by Purdue University Libraries Open Access Publishing Fund.

This work involved human subjects or animals in its research. Approval of all ethical and experimental procedures and protocols was granted by the Purdue University Institutional Review Board, under Application No. 1903021919, approved March 23, 2022.

Biographies

FOLK W. NARONGRIT (Member, IEEE) received the B.Eng. degree in electrical engineering, in 2020, specializing in power engineering and electronics and the M.S. degree in electrical engineering from the University of Southern California, LA, USA, in 2021. He is currently pursuing the M.S. degree in biomedical engineering and the Ph.D. degree in electrical and computer engineering with Purdue University, West Lafayette, IN, USA.

Since 2021, he has been a Research Assistant with the Magnetic Resonance Biomedical Engineering Laboratory (MRBEL), Purdue University. His research interest includes the development of magnetic resonance imaging hardware for clinical and research use.

Mr. Narongrit is an Ananda Mahidol Fellow and receives full funding from the Royal Thai Government. His awards and honors include the IEEE MTT-S Graduate Research Fellowship, Panasonic Engineering Fellow, and the Engineering Institute of Thailand Graduate Excellence Award.

THEJAS VISHNU RAMESH (Member, IEEE) received the B.E. degree in electronics and communication engineering from Visvesvaraya Technological University, Belagavi, Karnataka, India, in 2017. He is currently pursuing the Ph.D. degree in biomedical engineering with Purdue University, West Lafayette, IN, USA.

From 2018 to 2019, he was a RF Engineer with MR Coils BV, Zaltbommel, The Netherlands. He was a Lead Electrical Engineer with Philips, Pune, India, from 2020 to 2022. His research interests include developing wearable MRI receive arrays, parallel transmit/receive arrays, and other MRI hardware for clinical and ultra-high field MRI scanners.

JOSEPH V. RISPOLI (Member, IEEE) received the B.S. degree in electrical engineering from the University of Virginia, Charlottesville, VA, USA, in 2002, and the Ph.D. degree in biomedical engineering from Texas A&M University, College Station, TX, USA, in 2015. He was a Hardware Development Engineer with Dell Inc., from 2002 to 2010. He joined Purdue University, in 2015, and was promoted to an Associate Professor with the Weldon School of Biomedical Engineering and the Elmore Family School of Electrical and Computer Engineering, in 2022. He is currently an Associate Professor with the Department of Radiology and Medical Imaging, University of Virginia.

REFERENCES

[1]. Nishimura D, Principles of Magnetic Resonance Imaging, 1.2. Stanford, CA, USA: Stanford Univ., 2010.

[2]. Motovilova E, Tan ET, Taracila V, Vincent JM, Grafendorfer T, Shin J, Potter HG, Robb FJL, Sneag DB, and Winkler SA, "Stretchable self-tuning MRI receive coils based on liquid metal technology (LiquiTune)," Sci. Rep, vol. 11, no. 1, pp. 1–10, Aug. 2021, doi: 10.1038/s41598-021-95335-6. [PubMed: 33414495]

[3]. Ladd ME, Bachert P, Meyerspeer M, Moser E, Nagel AM, Norris DG, Schmitter S, Speck O, Straub S, and Zaiss M, "Pros and cons of ultra-high-field MRI/MRS for human application," Prog. Nucl. Magn. Reson. Spectrosc, vol. 109, pp. 1–50, Dec. 2018, doi: 10.1016/j.pnmrs.2018.06.001. [PubMed: 30527132]

[4]. Vaughan JT and Griffiths JR, RF Coils for MRI. Hoboken, NJ, USA: Wiley, 2012.

[5]. Cho Y, Basir A, and Yoo H, "Adjustable RF transmitter head coil: Improving transmit efficiency with SAR management for 7-T magnetic resonance imaging," IEEE Trans. Microw. Theory Techn, vol. 69, no. 5, pp. 2686–2696, May 2021, doi: 10.1109/TMTT.2021.3057620.

[6]. Winkler SA, Corea J, Lechêne B, O'Brien K, Bonanni JR, Chaudhari A, Alley M, Taviani V, Grafendorfer T, Robb F, Scott G, Pauly J, Lustig M, Arias AC, and Vasanawala S, "Evaluation of a flexible 12-channel screen-printed pediatric MRI coil," Radiology, vol. 291, no. 1, pp. 180–185, Apr. 2019, doi: 10.1148/radiol.2019181883. [PubMed: 30806599]

[7]. Frass-Kriegl R, de Lara LIN, Pichler M, Sieg J, Moser E, Windischberger C, and Laistler E, "Flexible 23-channel coil array for high-resolution magnetic resonance imaging at 3 Tesla," PLoS ONE, vol. 13, no. 11, Nov. 2018, Art. no. e0206963, doi: 10.1371/journal.pone.0206963.

[8]. Ruytenberg T, Webb A, and Zivkovic I, "Shielded-coaxial-cable coils as receive and transceive array elements for 7T human MRI," Magn. Reson. Med, vol. 83, no. 3, pp. 1135–1146, Mar. 2020, doi: 10.1002/mrm.27964. [PubMed: 31483530]

[9]. Hosseinnezhadian S, Frass-Kriegl R, Goluch-Roat S, Pichler M, Sieg J, Vít M, Poirier-Quinot M, Darrasse L, Moser E, Ginefri J-C, and Laistler E, "A flexible 12-channel transceiver array of transmission line resonators for 7 t MRI," J. Magn. Reson, vol. 296, pp. 47–59, Nov. 2018, doi: 10.1016/j.jmr.2018.08.013. [PubMed: 30205313]

[10]. Jia F, Yuan H, Zhou D, Zhang J, Wang X, and Fang J, "Knee MRI under varying flexion angles utilizing a flexible flat cable antenna," NMR Biomed, vol. 28, no. 4, pp. 460–467, Apr. 2015, doi: 10.1002/nbm.3264. [PubMed: 25740180]

[11]. Mager D, Peter A, Del Tin L, Fischer E, Smith PJ, Hennig J, and Korvink JG, "An MRI receiver coil produced by inkjet printing directly on to a flexible substrate," IEEE Trans. Med. Imag, vol. 29, no. 2, pp. 482–487, Feb. 2010, doi: 10.1109/TMI.2009.2036996.

[12]. Hardy CJ, Giaquinto RO, Piel JE, Rohling AAS KW, Marinelli L, Blezek DJ, Fiveland EW, Darrow RD, and Foo TKF, "128-channel body MRI with a flexible high-density receiver-coil array," J. Magn. Reson. Imag, vol. 28, no. 5, pp. 1219–1225, Nov. 2008, doi: 10.1002/jmri.21463.

[13]. Port A, Luechinger R, Albisetti L, Varga M, Marjanovic J, Reber J, Brunner DO, and Pruessmann KP, "Detector clothes for MRI: A wearable array receiver based on liquid metal in elastic tubes," Sci. Rep, vol. 10, no. 1, pp. 1–10, Jun. 2020, doi: 10.1038/s41598-020-65634-5. [PubMed: 31913322]

[14]. Nordmeyer-Massner JA, De Zanche N, and Pruessmann KP, "Stretchable coil arrays: Application to knee imaging under varying flexion angles," Magn. Reson. Med, vol. 67, no. 3, pp. 872–879, Mar. 2012, doi: 10.1002/mrm.23240. [PubMed: 22213018]

[15]. Vincent JM, Gim M, and Rispoli JV, "Elastically stretchable and flexible RF receive coils for magnetic resonance imaging," in Proc. Int. Conf. Electromagn. Adv. Appl. (ICEAA), Aug. 2021, p. 319, doi: 10.1109/ICEAA52647.2021.9539531.

[16]. Vincent JM and Rispoli JV, "Conductive thread-based stretchable and flexible radiofrequency coils for magnetic resonance imaging," IEEE Trans. Biomed. Eng, vol. 67, no. 8, pp. 2187–2193, Aug. 2020, doi: 10.1109/TBME.2019.2956682. [PubMed: 31794385]

[17]. Ramesh TV, Narongrit FW, Susnjar A, and Rispoli JV, "Stretchable receive coil for 7T small animal MRI," J. Magn. Reson, vol. 353, Aug. 2023, Art. no. 107510, doi: 10.1016/j.jmr.2023.107510.

[18]. Sieroń D, Jabłońska I, Lukoszek D, Szyluk K, Meusburger H, Delimpasis G, Kostrzewa M, Platzek I, and Christe A, "Knee diameter and cross-section area measurements in MRI as new promising methods of chondromalacia diagnosis-pilot study," Medicina, vol. 58, no. 9, p. 1142, Aug. 2022, doi: 10.3390/medicina58091142. [PubMed: 36143819]

[19]. Joshipura K, Muñoz-Torres F, Vergara J, Palacios C, and Pérez CM, "Neck circumference may be a better alternative to standard anthropo-metric measures," J. Diabetes Res, vol. 2016, pp. 1–8, Jan. 2016, doi: 10.1155/2016/6058916.

[20]. Kumar A, Edelstein WA, and Bottomley PA, "Noise figure limits for circular loop MR coils," Magn. Reson. Med, vol. 61, no. 5, pp. 1201–1209, May 2009, doi: 10.1002/mrm.21948. [PubMed: 19253376]

[21]. Mehmann A, Vogt C, Varga M, Port A, Reber J, Marjanovic J, Pruessmann KP, Sporrer B, Huang Q, and Tröster G, "Automatic resonance frequency retuning of stretchable liquid metal receive coil for magnetic resonance imaging," IEEE Trans. Med. Imag, vol. 38, no. 6, pp. 1420–1426, Jun. 2019, doi: 10.1109/TMI.2018.2888959.

[22]. Enríquez ÁG, Vincent JM, and Rispoli JV, "Dual-tuned removable common-mode current trap for magnetic resonance imaging and spectroscopy," in Proc. 41st Annu. Int. Conf. IEEE Eng. Med. Biol. Soc. (EMBC), Jul. 2019, pp. 6802–6805, doi: 10.1109/EMBC.2019.8857944.

[23]. Yang X, Zheng T, and Fujita H, "T/R switches, Baluns, and detuning elements in MRI RF coils," in Proc. Int. Soc. Mag. Reson. Med, 2006, pp. 1–7. Accessed: Sep. 8, 2022. [Online]. Available: https://cds.ismrm.org/protected/06MProceedings/

[24]. Ha Y, Selvaganesan K, Wu B, Hancock K, Rogers C, Hosseinnezhadian S, Galiana G, and Constable RT, "Practical method for RF pulse distortion compensation using multiple square pulses for low-field MRI," PLoS ONE, vol. 17, no. 9, Sep. 2022, Art. no. e0273432, doi: 10.1371/journal.pone.0273432.

[25]. Gruber B, Froeling M, Leiner T, and Klomp DWJ, "RF coils: A practical guide for nonphysicists," J. Magn. Reson. Imag, vol. 48, no. 3, pp. 590–604, Sep. 2018, doi: 10.1002/jmri.26187.

[26]. Medical Electrical Equipment: Particular Requirements for the Basic Safety and Essential Performance of Magnetic Resonance Equipment for Medical Diagnosis, document IEC 60601-2-33:2022, Int. Electrotechnical Commission, 4th ed., 2022.

[27]. Center for Devices and Radiological Health. (Dec. 2020). Magnetic Resonance (MR) Receive-Only Coil Performance Criteria for Safety and Performance-Based Pathway. U.S. Food and Drug Administration. [Online]. Available: https://www.fdanews.com/ext/resources/files/2019/12-06-19-MR-Coil-Safety-Guidance.pdf?1575657984

[28]. National Electrical Manufacturers Association. Characterization of Radiofrequency (RF) Coil Heating in Magnetic Resonance Imaging Systems, document NEMA MS 14–2019, 2019. [Online]. Available: https://www.nema.org/standards/view/Characterization-of-Radiofrequency-RF-Coil-Heating-in-Magnetic-Resonance-Imaging-Systems

[29]. Zanche ND. (Mar. 2020). ISMRM Best Practices for Safety Testing of Experimental RF Hardware. [Online]. Available: https://www.ismrm.org/safety/RF_Hardware_Safety_Testing_2022-03.pdf

[30]. Narongrit FW, Ramesh TV, and Rispoli JV, "Parametric design of a 3D-printed removable common-mode trap for magnetic resonance imaging," in Proc. IEEE MTT-S Int. Microw. Biomed. Conf. (IMBioC), Leuven, Belgium, Sep. 2023, pp. 127–129, doi: 10.1109/IMBioC56839.2023.10304882.

[31]. Determination of Signal-to-Noise Ratio (SNR) in Diagnostic Magnetic Resonance Imaging, document NEMA MS 1–2008 (R2014, R2020), National Electrical Manufacturers Association, 2021. [Online]. Available: https://www.nema.org/standards/view/Determination-of-Signal-to-Noise-Ratio-in-Diagnostic-Magnetic-Resonance-Imaging

[32]. U.S. Food and Drug Administration. FDA Discussion Paper: 3D Printing Medical Devices and the Point of Care. Accessed: Dec. 9, 2023. [Online]. Available: https://www.fda.gov/media/154729/download

[33]. Talkington K. FDA's Regulatory Framework for 3D Printing of Medical Devices at the Point of Care Needs More Clarity. Accessed: Dec. 9, 2023. [Online]. Available: https://pew.org/3zkHsSS

[34]. Obradov M, Bénard MR, Janssen MMA, Anderson PG, Heesterbeek PJC, and Spruit M, "Kinematic magnetic resonance imaging assessment of the degenerative cervical spine: Changes after anterior decompression and cage fusion," Global Spine J., vol. 6, no. 7, pp. 673–678, Nov. 2016, doi: 10.1055/s-0036-1579551. [PubMed: 27781187]

[35]. Motovilova E, Ching T, Vincent J, Shin J, Tan ET, Taracila V, Robb F, Hashimoto M, Sneag DB, and Winkler SA, "Dual-channel stretchable, self-tuning, liquid metal coils and their fabrication techniques," Sensors, vol. 23, no. 17, p. 7588, Sep. 2023, doi: 10.3390/s23177588. [PubMed: 37688046]

[36]. Muftuler LT, Gulsen G, Sezen KD, and Nalcioglu O, "Automatic tuned MRI RF coil for multinuclear imaging of small animals at 3T," J. Magn. Reson, vol. 155, no. 1, pp. 39–44, Mar. 2002, doi: 10.1006/jmre.2002.2510. [PubMed: 11945031]

[37]. Venook RD, Hargreaves BA, Gold GE, Conolly SM, and Scott GC, "Automatic tuning of flexible interventional RF receiver coils," Magn. Reson. Med, vol. 54, no. 4, pp. 983–993, Oct. 2005, doi: 10.1002/mrm.20616. [PubMed: 16155871]

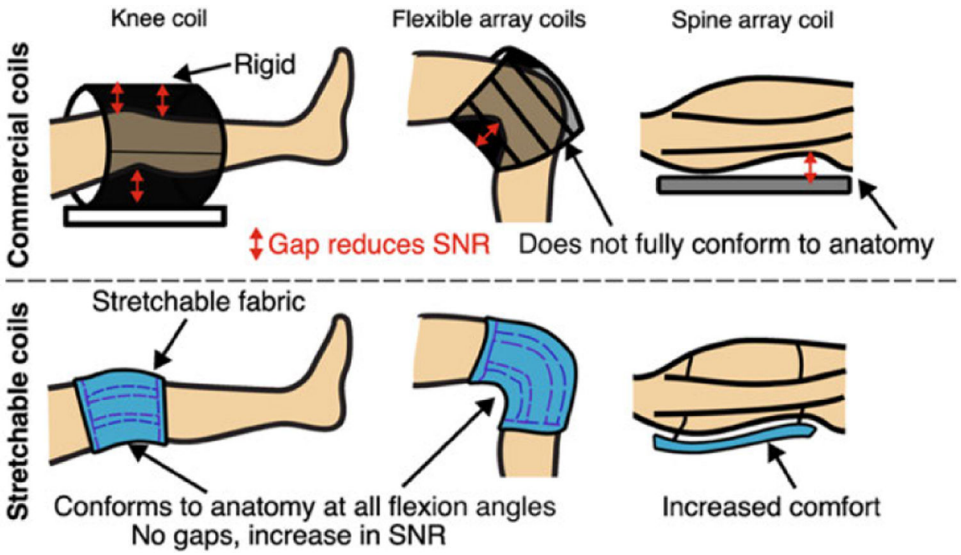

FIGURE 1.

A comparison between commercial arrays (top) and the proposed stretchable array (bottom). Conventional rigid arrays are fixed in size. A large gap between the anatomy and coil array lowers SNR. Commercial flexible arrays, while it provides a closer fit, it is still relatively rigid, resulting in a tradeoff between conformity and comfort. Our stretchable array closely conforms to the shape of the curved anatomy while using soft fabric material, yielding high SNR and patient comfort.

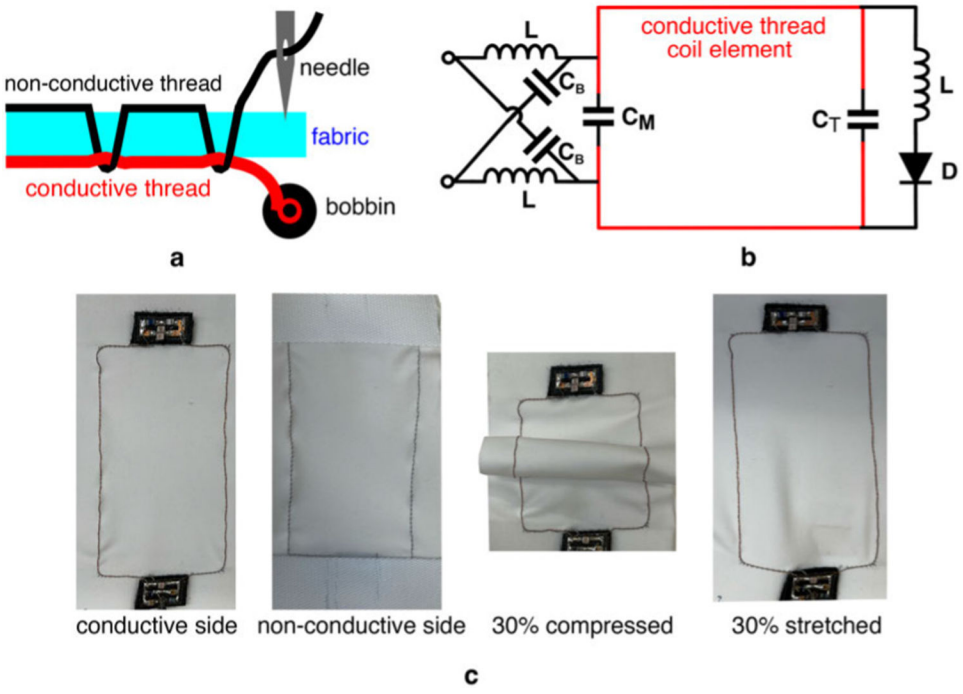

FIGURE 2.

(a) The embroidery process contains the conductive thread in the lower half of the machine (bobbin) and a standard non-conductive thread in the needle. (b) Schematic of the stretchable coil showing the tuning (CT), match (CM), and balun (CB) capacitors, the diode (D), and the inductor (L). (c) Photograph of one coil element at various stretch and compression.

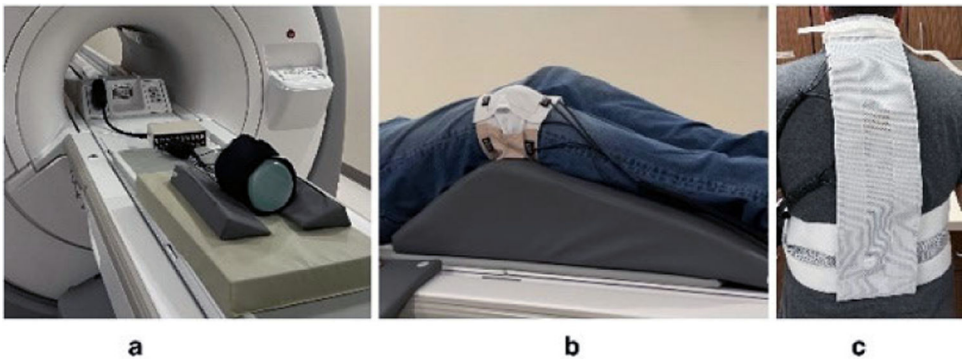

FIGURE 3.
Experimental setup. (a) Phantom imaging setup (b) Knee imaging at 15-degree flexion (c) Stretchable coil as a spine array.

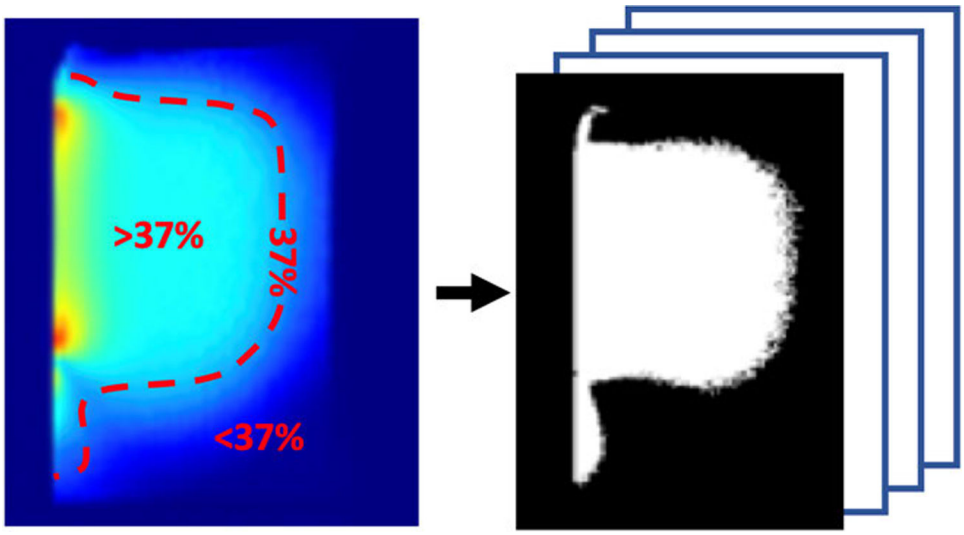

FIGURE 4.

Depiction of the computation of the sensitive volume. A masking threshold removes pixels with less than 37% sensitivity (relative to the center of the coil). Then the remaining pixel area is computed, then the same is performed for the other slices.

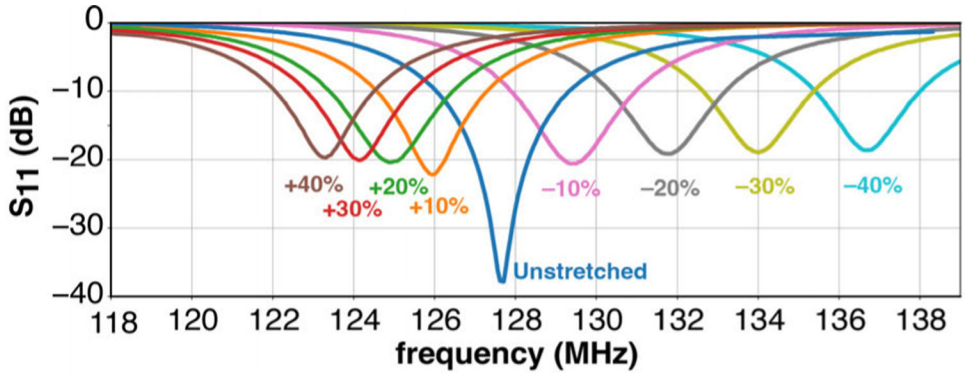

FIGURE 5.
Return loss (S_{21}) of the coil showing the effects of stretch on the resonance frequency shift.

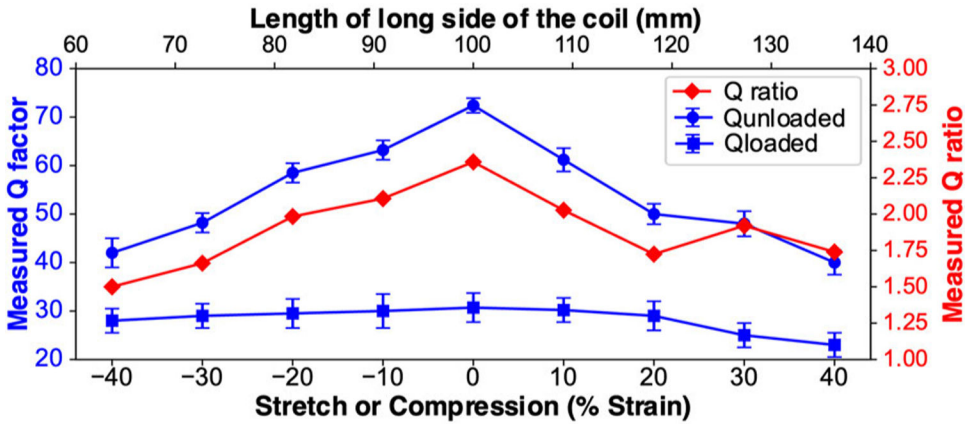

FIGURE 6.

Measured loaded Q_{loaded} and unloaded Q_{unloaded} quality factors of the stretchable coil at various uniform strain and their corresponding Q ratio $Q_{\text{unloaded}}/Q_{\text{loaded}}$.

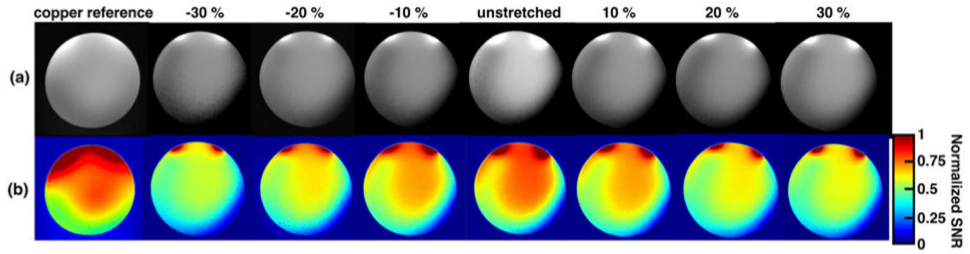

FIGURE 7.

Phantom tests with the proposed coil compared to the reference coil (a) MR images of a single stretchable coil element at various stretch and compression. (b) SNR map normalized to the global maximum SNR.

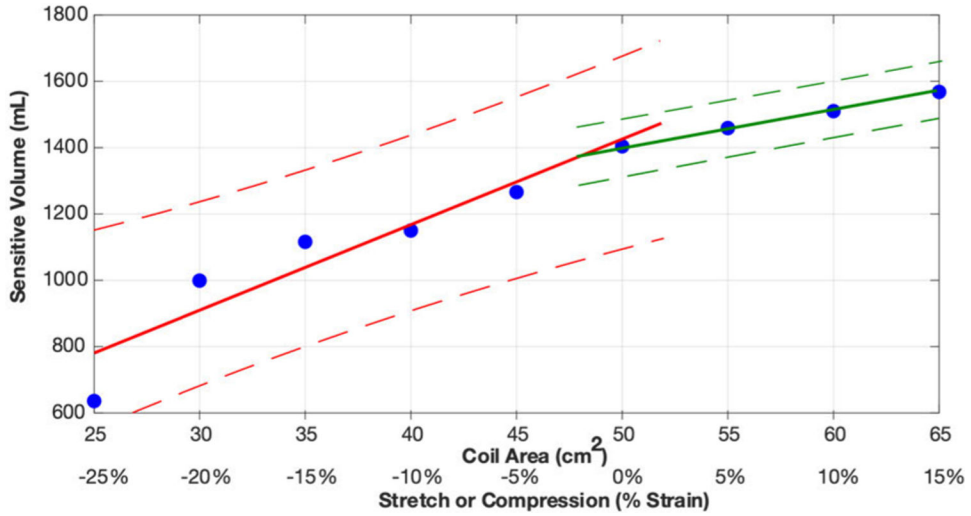

FIGURE 8.

Sensitive volume changes with respect to stretched or compressed coil area. The line of best fit and 95% confidence interval of the fit is given for stretch and compression separately. Compression (red): Sensitive Volume = 25.40 (Coil Area) + 134 with $r^2 = 0.8970$; Stretch (green): Sensitive Volume = 10.93 (Coil Area) + 857.33 with $r^2 = 0.9997$.

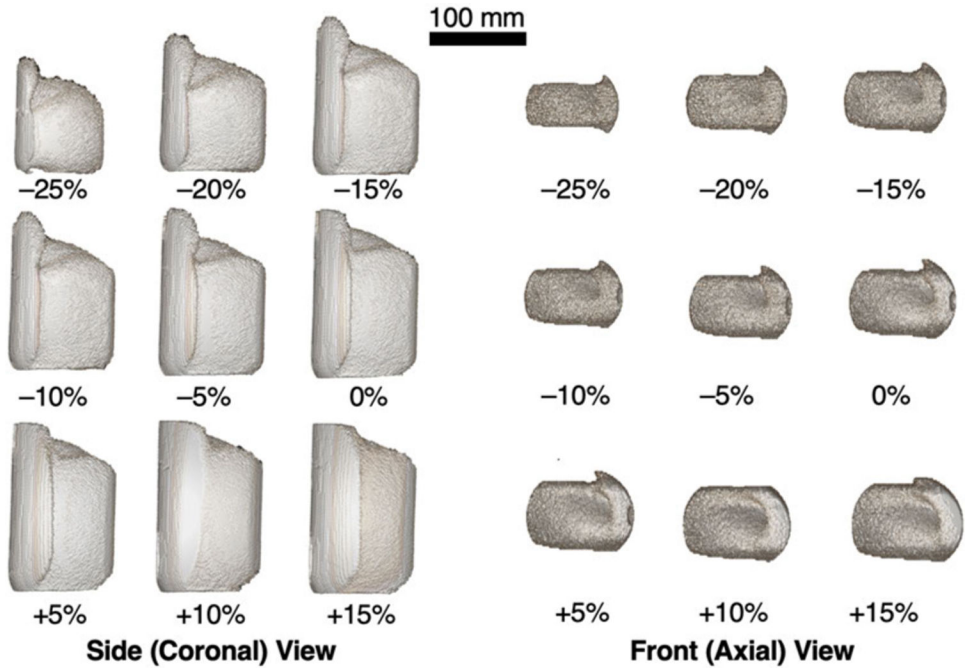

FIGURE 9.
Three-dimensional visualization of sensitive volume changes for each stretch and compression.

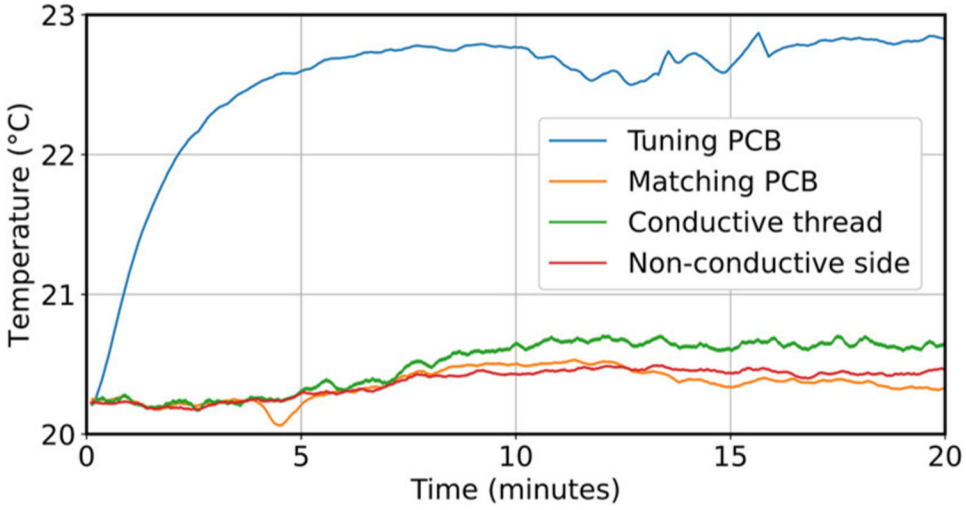

FIGURE 10.

Temperature data of the stretchable coil and its components during the first 20 minutes of the temperature safety test scan for the Normal intended use, phantom loaded, isocenter configuration. The full temperature data for all eight configurations are available in Supplementary Fig. 1.

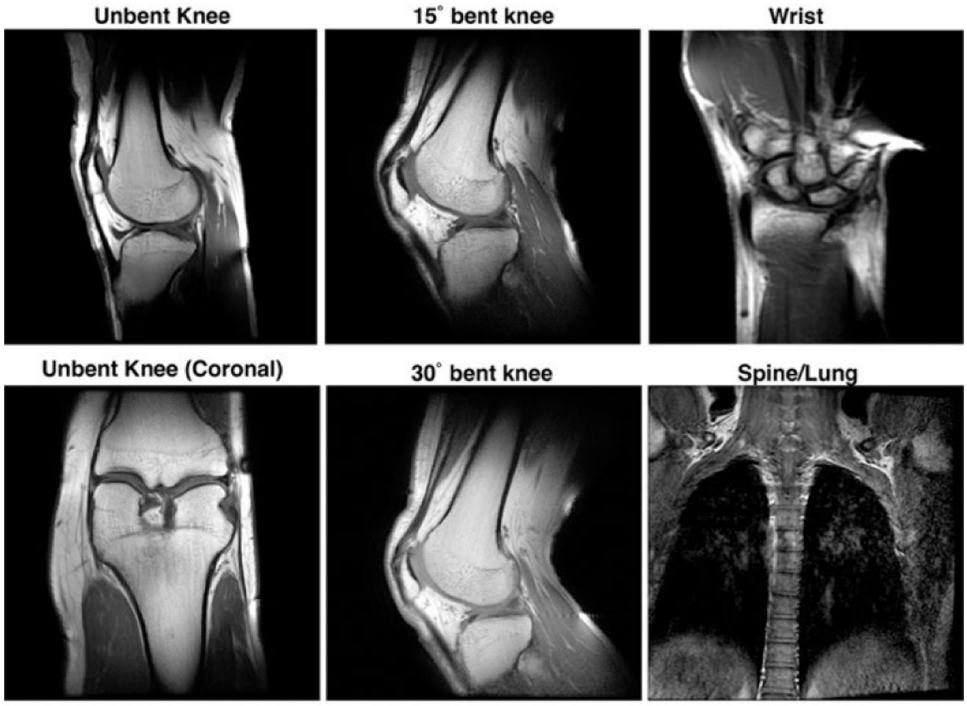

FIGURE 11.
Select MRI scans from in vivo experiments.